19th International Conference on
Adaptive Structures and Technologies
October 6-9, 2008
Ascona, Switzerland

Experimental and parametric analysis of corrugated composite structures for morphing skin applications

Christophe Thill[1], Julie A Etches[2], Ian P Bond[3]*, Paul M Weaver[4] & Kevin D Potter[5]
[1] PhD student, University of Bristol, UK
[2] Research Associate, University of Bristol, UK
[3]* Reader in Aerospace Materials, Advanced Composites Centre for Innovation and Science (ACCIS), University of Bristol, Department of Aerospace Engineering, Queen's Building, University Walk, Bristol, BS8 1TR. UK, Tel: +44 (0)117 928 8662, Fax: + 44 (0)117 927 2771, Email: I.P.Bond@bristol.ac.uk
[4] Reader in Lightweight Structures, University of Bristol, UK
[5] Reader in Composites Manufacture, University of Bristol, UK

ABSTRACT

One potential solution for a morphing wing concept could make use of a skin panel that incorporates corrugated laminates in a sandwich structure. Located in the trailing edge region it would have low in- and out-of-plane stiffness in the wing chordwise direction in order to achieve large camber and chord length changes on a morphing aerofoil section. This investigation presents experimental and analytical results for a sandwich structure with trapezoidal corrugated skins. Furthermore, a parametric study analyses the effects of corrugation geometry and form on the structural elastic strain and equivalent elastic tensile modulus transversely to the corrugation direction. The results give a good indication of the wide envelope within which corrugated laminates can be designed to meet the requirements for a morphing skin application.

Keywords: morphing, skins, corrugations, composites

NOMENCLATURE

A: extensional rigidity/stiffness, [N/m]
a: specimen width, [m]
b_1: top horizontal hat-type corrugation length, [m]
b_2: vertical/inclined hat-type corrugation length, [m]
b_3: bottom horizontal hat-type corrugation length, [m]
D: flexural rigidity/stiffness, [Nm]
d: sandwich structure thickness, [m]
E: tensile elastic modulus, [Pa]
e: length of sandwich foam section, [m]
f: offset of load application during bending test, [m]
h: corrugation height, [m]
k: stiffness, [N/m]
k_b: bending constant of sinusoidal corrugation, [m]
k_t: tensile constant of sinusoidal corrugation, [m]
L: specimen gauge length, [m]
l_{cor}: corrugated section length of sandwich structure, [m]
r: radius of round corrugation, [m]
s: half developed length of sinusoidal corrugation, [m]
t: cured laminate thickness, [m]
u: displacement, [m]
V_f: fibre volume fraction, [%]
W: applied load/weight, [N]
w: half wavelength of sinusoidal corrugation, [m]
ε: strain, [-]
v: Poisson's ratio, [-]
Φ: corrugation angle, [rad]
ρ: cured laminate density, [kg/m^3]
$()_{equ}$: relating quantity to the equivalent property
$()_{exp}$: relating to the experimentally measured value
$()_F$: relating to flexure
$()_T$: relating to tension
$()_{yy}$: relating to global yy-direction
$()_{zz}$: relating to global zz-direction
$()^{hat}$: relating to hat-type corrugations
$()^{rou}$: relating to round corrugations
$()^{san}$: relating to sandwich structure
$()^{sin}$: relating to sinusoidal corrugations
$()^{tra}$: relating to trapezoidal corrugations

1. INTRODUCTION

Morphing wing technology has received increased attention, both in industry and academia, over the last decade since their advantages over conventional aircraft wings have been shown. Three likely major benefits are: aerodynamic efficiency improvements, flight envelope expansion and increased mission capability. Many concepts have focused on radically changing the structure and layout of wings to accommodate large changes in camber and surface area. Although these ideas are beneficial to progress the technology in the long term, they are immature at present and thus unlikely to have an immediate impact [1]. Hence, subtle modifications using well known materials and features may bring small but steady improvements more rapidly. Introducing novel materials step by step will eventually lead to overall revolutionary innovations in a more controlled and possibly safer approach.
Current trailing edge control surfaces, e.g. ailerons and flaps, are hinged and/or linked to the main wing and actuated hydraulically or mechanically [2]. This system brings about discontinuities in the wing profile, both chordwise and spanwise, in the form of gaps and large sudden geometric changes. While the chordwise discontinuities can be beneficial, in terms of preventing flow separation [3], the spanwise ones are generally detrimental to the aerodynamic efficiency. Furthermore, the high-lift systems, e.g. flaps and slats, can be very complex which increases weight, assembly, maintenance and operational costs. One aspiration of morphing is to avoid the wing discontinuities and possibly simplify actuating mechanisms [4]. The aerodynamic and flight envelope advantages of these seamless variable camber wings have been shown in programs such as the Mission Adaptive Wing (MAW) and DARPA (Defense Advanced Research Projects Agency) Smart Wing. However, the MAW programme's actuation system was too heavy and complex to offset the aerodynamic benefits while the Smart Wing project relied on novel actuation methods that lacked the level of maturity to perform in full-scale flight testing. Note that in both these cases the actuation system was contained inside the control surface reducing the drag significantly [5-8].
A variable camber and chord length aerofoil might be designed by the application of a morphing seamless trailing edge concept (see Figure 1). This introduces particular challenges at the wing skin level as highly anisotropic properties are required. The aim of this study (part of the SMARTCOMP University Strategic Technology Partnership with GE Aviation) was to develop a novel concept using typical airframe materials that could replace a conventional mechanical hinged control surface at the trailing edge of a small aircraft.
The project has identified corrugated laminates as a possible solution. They are extremely anisotropic as they are very stiff parallel to the corrugation direction but compliant in the perpendicular direction. Corrugated structures in general are not new to the engineering or natural world and have been used over many decades in civil, naval, automotive and aerospace applications due to their efficient performance i.e. low mass to stiffness (along corrugations) ratio [9-11]. In nature, numerous insects, such as the damselfly, desert locust and dragonfly, have corrugated wings for deployable mechanisms, stiffness requirements and/or aerodynamic effects [12-16]. Yokozeki et al [17] were among the first to suggest corrugated laminates made from carbon/epoxy composites for morphing wings. A similar study was carried out subsequently by Thill et al [18]. The corrugations were aligned in the wing's spanwise direction hence giving low axial and flexural stiffnesses in the chordwise direction to allow for trailing edge camber changes and extensions, whilst providing high stiffness to withstand structural and aerodynamic loads in the spanwise direction.
Although this high degree of anisotropy is generally beneficial for morphing the structural integrity in chordwise bending of corrugated laminates is possibly too low for them to support the aerodynamic loads when acting as a wing skin panel. Hence in this study corrugated laminates have been incorporated into a composite sandwich structure and it is suggested that this type of configuration could be deployed as a skin panel in the trailing edge region (about 70% chord) of a small aircraft, e.g. unmanned aerial vehicle wing.

Figure 1: Aerofoil with conventional hinged (top) and variable camber corrugated control surface (bottom)

This arrangement will bridge the discontinuities that normally exist between a conventional control surface and wing (see Figure 1), and increase the chordwise bending stiffness compared to single corrugated laminates. This paper presents the practical methodology in terms of both the manufacturing and experimental testing of a single unit cell of corrugated sandwich structure. The principle being that a single unit cell will only give small displacements but combining many of these will result in an overall large displacement. The main thrust of the work goes on to consider the analysis of fibre reinforced composite corrugated laminates of various geometries and forms (trapezoidal, rectangular, triangular, re-entrant (hat-type), sinusoidal and round). They could all be used for morphing skin applications as part of a composite sandwich structure depending on the stiffness and displacement requirements. Using analytical and computational methods the equivalent elastic tensile modulus and strain of the differing corrugated laminates were derived and compared to develop the design space for applications using corrugated laminates.

2. METHODOLOGY

2-1. Specimen manufacturing

The corrugated laminates were manufactured in the same way as described in the initial study on corrugated laminates by Thill et al. [18]. For this study only two trapezoidal corrugation waves were incorporated between flat outer sections. The preimpregnated tape used was made from woven glass fibres (5 harness satin weave) in an epoxy matrix (Cycom® 977-2 by CYTEC). Table 1 lists the cured material and nominal trapezoidal geometric properties. Two laminates were made per sandwich structure panel. The laminates were then bonded to a foam core (Rohacell® 31) using a two part epoxy paste adhesive (Redux 810 by HEXCEL COMPOSITES). To accelerate the cure of the adhesive the assembled sandwich structure was put in an oven for 1 hour at 70°C. The final sandwich panel is shown in Figure 2. It has nominal projected dimensions of 210 x 101.5 x 13mm. Each panel was then cut into the final specimen size of 25mm width using a diamond saw. The cross-section of a specimen is shown in Figure 2. The final step involved bonding 0°/90° glass/epoxy laminate end tabs (nominal dimensions of 25 x 25 x 2.5mm) onto the sandwich skin panels using the same adhesive as previously.

Table 1: Cured material and nominal trapezoidal geometric properties of corrugated laminate

			V_f*	ρ*	$E_T^{\#}$	$E_F^{\#}$		**Φ**	[deg]	30		b_3	[mm]	5.0
Fibre type	**Weave**	**Resin**	**[%]**	**[kg/m^3]**	**[GPa]**	**[GPa]**		**h**	[mm]	5.0		**a**	[mm]	25.0
Glass	5 harness satin	Cytec 977-2	42.7%	2080	23.3	13.3		b_1	[mm]	5.0		**t**	[mm]	0.5
* data from manufacturer, # data from experiment												b_2	[mm]	5.8

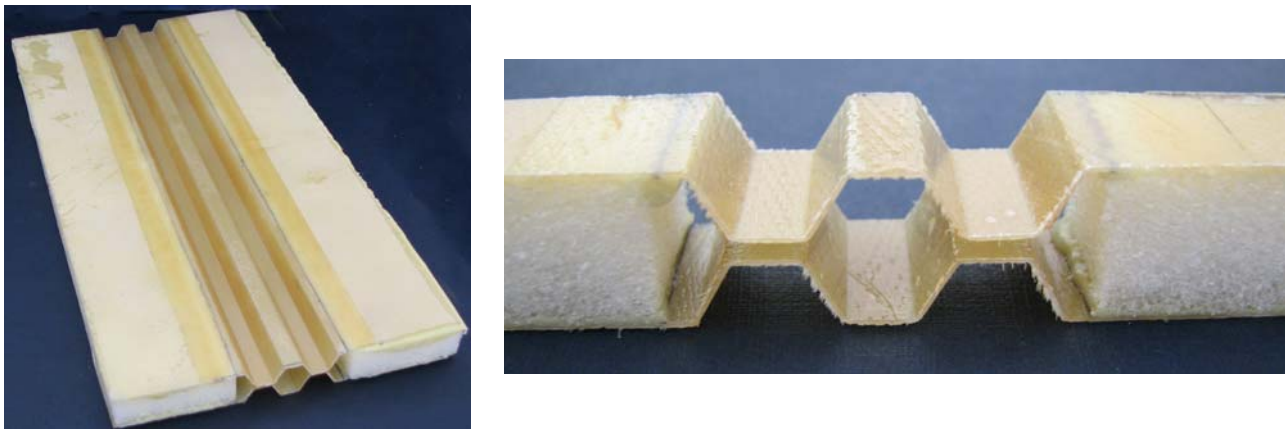

Figure 2: Corrugated sandwich structure in panel form (left) and specimen form (right)

2-2. Experimental studies

Two experimental tests were performed to quantify the elastic tensile and bending stiffnesses of the sandwich structure (see Figure 3). Five specimens were used for each test. First a tensile test was completed in an Instron 3343 with a load cell of 1kN; cross-head displacements and loads were recorded. Secondly a cantilever bending test was carried out by clamping the specimens onto a rigid A-frame at one end and hanging weights from the other end (the weights were offset by a distance f=45mm from the specimen edge) using Dyneema® fibre and a slotted weight hanger. The weights were recorded manually and the axial displacements were measured with a video extensometer. This system uses a SONY XCD-X710 digital video camera with a COMPUTAR zoom lens (18-108/2.5) connected to a computer running "Video Gauge" software by IMETRUM. The software is able to track the displacement of targets marked on the specimen during the testing. A reference distance is used so that displacements and distances output by the software in pixels can be readily converted into actual metric values.

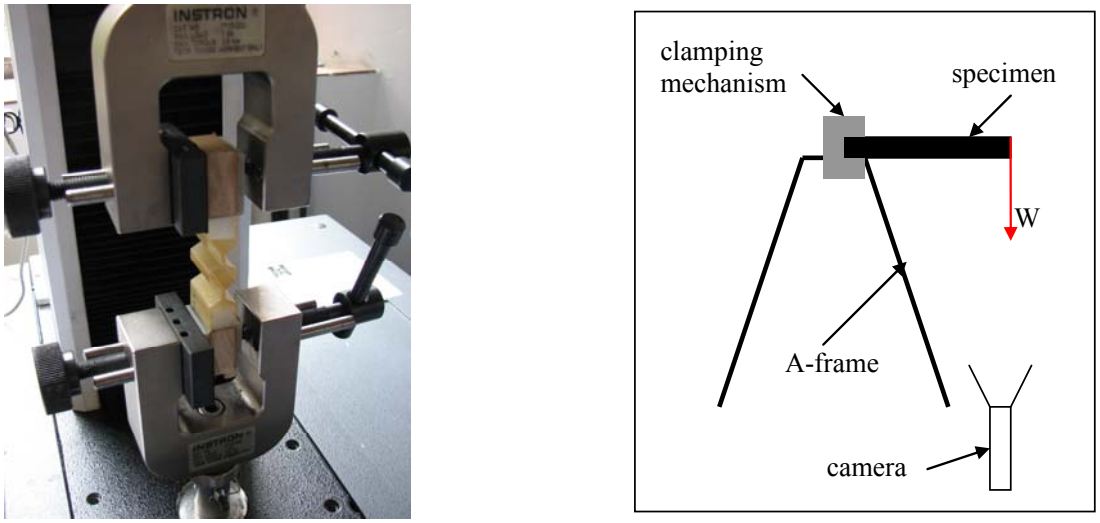

Figure 3: Experimental testing set-up - tension (left) and cantilever bending (right)

2-3. Experimental data analysis

The equivalent tensile elastic modulus of the sandwich structure measured transversely to the corrugation direction was calculated according to equation (1). Similarly, the equivalent flexural stiffness modulus of the sandwich structure measured transversely to the corrugation direction was

calculated according to equation (2).

$$\left(E_{yy}\right)_{equ,\exp}^{san} = \frac{W}{ad}\frac{L}{u_{yy}} \qquad (1)$$

$$\left(D_{yy}\right)_{equ,\exp}^{san} = \frac{1}{a\left(1-\nu_{12}^2\right)}\frac{W}{u_{zz}}\left[\frac{(L+f)L^2}{2} - \frac{L^3}{6}\right] \qquad (2)$$

2-4. Analytical models for corrugated laminates

Various analytical models that allow the prediction of the transverse equivalent (i.e. based on laminate thickness not projected dimension in x-z plane) elastic tensile modulus, stiffness and axial deflections of corrugated laminates of different corrugation forms exist in the literature. They are derived via strain energy principles and Castigliano's second theorem. Table 2 to Table 4 give the final expressions for the various corrugation forms and the notation for the geometry. Note that the models have been modified slightly both in terms of notation and modelling to suit this study. Bending and tensile effects in the corrugation members are considered while shear effects are neglected which is valid for the thin laminates considered herein. The buckling failure mode has also been neglected which might become important at high loads for thin laminates. Note that for the sinusoidal corrugations the tensile and bending constants, k_t and k_b respectively, need to be evaluated numerically for an accurate overall result. It was found that the assumption made by Briassoulis [19] to approximate $\cos(\pi/2-\Phi)$ by w/s is only good for small angles of $(\pi/2-\Phi)$ i.e. shallow sinusoidal corrugations or where $\tan(\pi/2-\Phi) \approx (\pi/2-\Phi)$.

Table 2: Analytical expressions for trapezoidal, rectangular, triangular and re-entrant corrugations [20]

Corrugation form: trapezoidal for 0°<Φ<90° - rectangular for Φ=0° - triangular for $b_1=b_3=0$ – re-entrant for -90°>Φ>0°

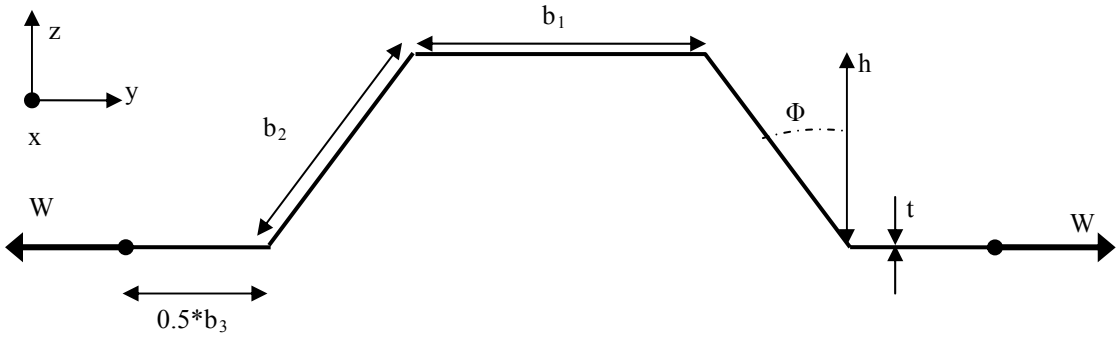

$$\left(E_{yy}\right)_{equ}^{hat} = \frac{E_T\left(b_1+2b_2\sin(\phi)+b_3\right)}{t\left(\frac{3h^2}{t^3}\left(b_1+b_3\right)+\frac{b_1+b_3}{t}+\frac{2b_2^3\cos^2(\phi)}{t^3}+\frac{2b_2\sin^2(\phi)}{t}\right)} \qquad (3)$$

$$\left(A_{yy}\right)_{equ}^{hat} = \frac{E_T}{1-\nu_{12}^2}\frac{\left(b_1+2b_2\sin(\phi)+b_3\right)}{\left(\frac{3h^2}{t^3}\left(b_1+b_3\right)+\frac{b_1+b_3}{t}+\frac{2b_2^3\cos^2(\phi)}{t^3}+\frac{2b_2\sin^2(\phi)}{t}\right)} \qquad (4)$$

$$\left(u_{yy}\right)^{hat} = \frac{W}{E_T}\left[\frac{3h^2}{at^3}\left(b_1+b_3\right)+\frac{b_1+b_3}{at}+\frac{2b_2^3\cos^2(\phi)}{at^3}+\frac{2b_2\sin^2(\phi)}{at}\right] \qquad (5)$$

Table 3: Analytical expressions for sinusoidal corrugations [19]

Corrugation form: sinusoidal

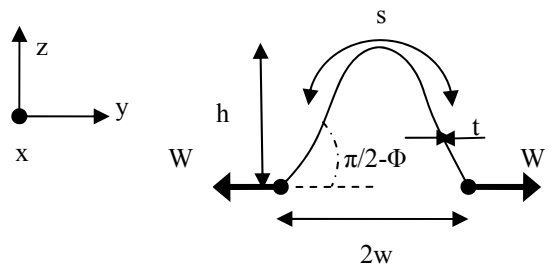

$$\left(E_{yy}\right)_{equ}^{\sin} = \frac{E_T w}{k_t + 3k_b\left(\frac{h}{t}\right)^2} \qquad (6)$$

$$\left(A_{yy}\right)_{equ}^{\sin} = \frac{E_T w}{k_t + 3k_b\left(\frac{h}{t}\right)^2}\frac{t}{\left(1-\nu_{12}^2\right)} \qquad (7)$$

$$\left(u_{yy}\right)^{\sin} = \frac{2W}{E_T at}\left(k_t + 3k_b\left(\frac{h}{t}\right)^2\right) \qquad k_t = \int_0^w \cos\left(\frac{\pi}{2}-\phi\right)dy$$

$$\frac{\pi}{2}-\phi = A\tan\left(\frac{\pi h}{2w}\cos\left(\frac{y\pi}{w}+\frac{3\pi}{2}\right)\right) \qquad k_b = \int_0^w \frac{1}{\cos\left(\frac{\pi}{2}-\phi\right)}\left(\sin\left(\frac{y\pi}{w}+\frac{3\pi}{2}\right)\right)^2 dy \qquad (8)$$

Table 4: Analytical expressions for round corrugations [17]

Corrugation form: round

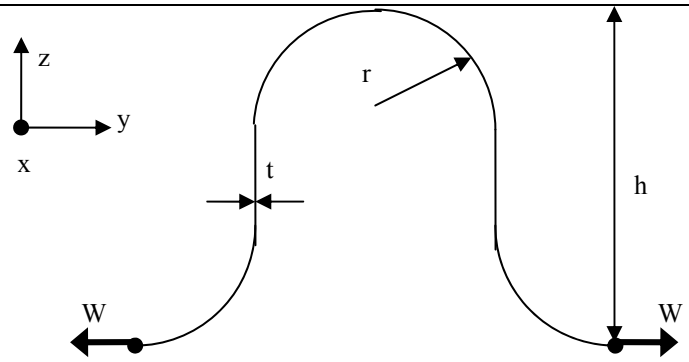

$$\left(E_{yy}\right)_{equ}^{rou} = \frac{E_T t^3}{12}\frac{r}{t}\frac{1}{\left[\frac{1}{3}\left(\frac{h-2r}{2}\right)^3 + r\left(\frac{\pi}{4}\left(2\left(\frac{h-2r}{2}\right)^2 + r^2 + \frac{t^2}{12}\right) + 2\left(\frac{h-2r}{2}\right)r\right)\right]} \qquad (9)$$

$$\left(A_{yy}\right)_{equ}^{rou} = \frac{E_T t^3}{12\left(1-\nu_{12}^2\right)^2}\frac{r}{\left[\frac{1}{3}\left(\frac{h-2r}{2}\right)^3 + r\left(\frac{\pi}{4}\left(2\left(\frac{h-2r}{2}\right)^2 + r^2 + \frac{t^2}{12}\right) + 2\left(\frac{h-2r}{2}\right)r\right)\right]} \qquad (10)$$

$$\left(u_{yy}\right)^{rou} = \frac{12W}{E_T at^3}4\left[\frac{1}{3}\left(\frac{h-2r}{2}\right)^3 + r\left(\frac{\pi}{4}\left(2\left(\frac{h-2r}{2}\right)^2 + r^2 + \frac{t^2}{12}\right) + 2\left(\frac{h-2r}{2}\right)r\right)\right] \qquad (11)$$

Additionally, for this study the transverse equivalent flexural stiffness is needed for the trapezoidal corrugated laminates given in equation (12), previously published by Rao [21] and Samanta & Mukhopadhyay [20].

$$\left(D_{yy}\right)_{equ}^{hat} = \frac{E_F t^3 \left(\frac{b_1}{2} + b_2 \sin(\phi) + \frac{b_3}{2}\right)}{12\left(1-\nu_{12}^2\right)\left(\frac{b_1}{2} + b_2 + \frac{b_3}{2}\right)} \qquad (12)$$

The analytical models in equations (3) to (12) have been validated with experimental and finite element analysis results by the authors and by the workers previously referenced.

2-5. Analytical model for corrugated sandwich structure

Since both the tensile and flexural stiffnesses of single trapezoidal corrugated laminates can be predicted analytically (see section 2-4.), the equivalent stiffnesses of the corrugated sandwich structure can also be derived. Figure 4 shows a schematic of the cross-section of the manufactured and tested specimen. Note that in principle the corrugated skins could be of any of the corrugation forms presented earlier.

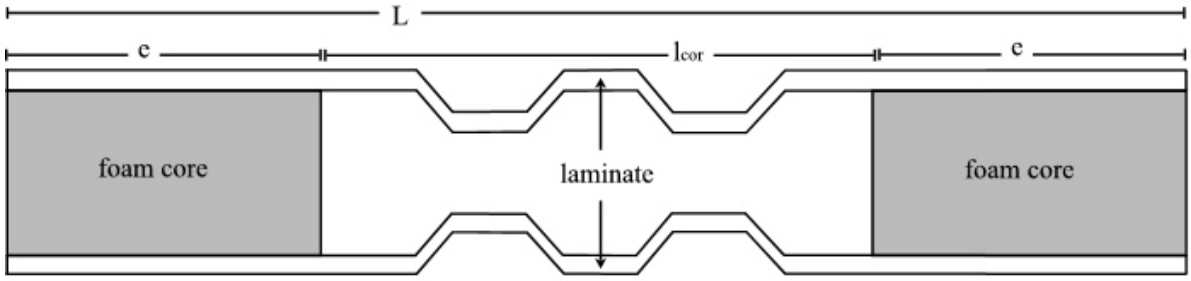

Figure 4: Schematic of cross-section of corrugated sandwich structure specimen

It is assumed that the conventional sandwich structure sections (with core) left and right of the corrugated section (without core) are fairly stiff and have no effect on the overall equivalent tensile modulus at low strains. Hence, only the centre section needs to be considered which consists of two trapezoidal corrugated laminates which can be considered as springs in parallel. The equivalent stiffness for such an arrangement is obtained by adding together the individual stiffnesses [22]. The stiffness of each spring (or corrugated laminate) is given by equation (13).

$$k_{equ}^{hat} = \frac{\left(E_{yy}\right)_{equ}^{hat} at}{l_{cor}} \qquad (13)$$

The equivalent tensile elastic modulus of the corrugated sandwich structure transverse to the corrugation direction is then derived as shown in equation (14). Note that the equivalent stiffness of the sandwich structure is based on its total thickness while the equivalent stiffness of the corrugated laminate is based on the laminate thickness only.

$$
\begin{aligned}
& k_{equ}^{san} = 2k_{equ}^{hat} \\
& \Leftrightarrow \frac{\left(E_{yy}\right)_{equ}^{san} ad}{L} = 2\frac{\left(E_{yy}\right)_{equ}^{hat} at}{l_{cor}} \\
& \Leftrightarrow \left(E_{yy}\right)_{equ}^{san} = \left(E_{yy}\right)_{equ}^{hat} \frac{2tL}{dl_{cor}}
\end{aligned}
\qquad (14)
$$

To predict the flexural rigidity of the corrugated sandwich structure it is assumed, as for the tensile case, that the sections outside of the two parallel corrugated laminates (see Figure 4) do not contribute to the bending stiffness of the total structure. The prediction of the flexural rigidity of the transverse corrugated sandwich structure is given in equation (15). Note that the factor accounting for total specimen length is based on equation (2) and the second moment of area has been estimated using the parallel axis theorem as stated in (15).

$$
\begin{aligned}
& \left(D_{yy}\right)_{equ}^{san} = \frac{1}{a\left(1-\nu_{12}^2\right)}\left(E_{yy}\right)_{equ}^{hat} I_{yy}^{san} \times factor\ accounting\ for\ total\ specimen\ length \\
& \Leftrightarrow \left(D_{yy}\right)_{equ}^{san} = 2\frac{1}{a\left(1-\nu_{12}^2\right)}\left(E_{yy}\right)_{equ}^{hat}\left[\left(I_{yy}\right)_{equ}^{hat} + area\times length^2\right]\left(\frac{2L^3}{3Ll_{cor}^2 - l_{cor}^3 + 6Ll_{cor}e - 3l_{cor}^2 e}\right) \\
& \Leftrightarrow \left(D_{yy}\right)_{equ}^{san} = 2\left[\left(D_{yy}\right)_{equ}^{hat} + \frac{\left(E_{yy}\right)_{equ}^{hat}}{a\left(1-\nu_{12}^2\right)} area\times length^2\right]\left(\frac{2L^3}{3Ll_{cor}^2 - l_{cor}^3 + 6Ll_{cor}e - 3l_{cor}^2 e}\right) \\
& where\ area\times length^2 = \frac{at}{l_{cor}}\left[2b_1\left(\frac{d}{2}-\frac{t}{2}\right)^2 + 2b_1\left(\frac{d}{2}-h-\frac{t}{2}\right)^2 + 4b_2\tan\phi\left(\frac{d}{2}-\frac{h}{2}-\frac{t}{2\cos\phi}\right)^2\right]
\end{aligned}
\qquad (15)
$$

3. RESULTS & DISCUSSION

3-1. Experimental, analytical and numerical results of corrugated sandwich structure

The experimental data for the tensile and bending tests for the five specimens are given in Figure 5. The tests were carried out up to failure for the tensile and in the linear elastic regime for the bending tests. The experimental, analytical and numerical results of a single trapezoidal corrugated laminate and the sandwich structure with trapezoidal corrugated skins, as shown in Figure 4, are given in Table 5. Both the transverse equivalent elastic moduli and bending stiffnesses are listed. The experimental data for the single trapezoidal laminate has been published previously by Thill et al. [18]. The analytical bending stiffnesses are based on the flexural modulus of the flat glass/epoxy laminate as given by Table 1. The numerical results were computed using two-dimensional beam elements in Abaqus/CAE (version 6.6-1) finite element analysis software.

These results show that the equivalent stiffness of these structures is very low in the direction transverse to the corrugations and can be several orders of magnitude lower than the stiffness longitudinal to the corrugation direction [18]. This makes them good candidate structures for morphing skins. Overall, experimental, analytical and numerical results agree reasonably well. The larger discrepancies in the bending stiffness are attributed to the difficulty in measuring them accurately with the available equipment and in the sandwich structure experimental stiffnesses are attributed to misalignments of the corrugated sandwich skins and loading, and variations in flat laminate material properties.

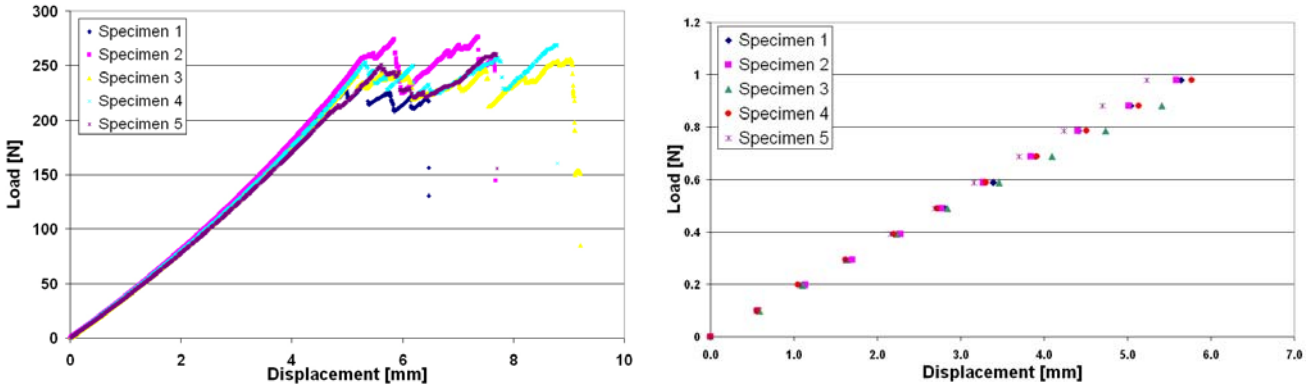

Figure 5: Experimental results of corrugated sandwich structure in tension (left) and in cantilever bending (right)

Table 5: Experimental and analytical results of trapezoidal corrugated laminates and sandwich structure

			Experimental		Analytical	Numerical
Type	Property	Unit	results	coefficient of variation	results	results
tra	$(E_{yy})_{equ}$	[MPa]	83.45	9.0%	88.09	86.48
	$(D_{yy})_{equ}$	[Nm]	0.16	8.2%	0.11	0.18
san	$(E_{yy})_{equ}$	[MPa]	7.03	4.0%	11.07	10.57
	$(D_{yy})_{equ}$	[Nm]	0.87	5.0%	1.39	1.43

3-2. Parametric study of single corrugated laminates

While section 3-1. and the previous study [18] on corrugated laminates experimentally demonstrated the anisotropy of corrugated laminates and the effects of material and corrugation geometry on stiffness, this study demonstrates analytically the effects of geometric parameters and corrugation forms on the structural strain and transverse equivalent modulus. As an example of the effect of geometry, a parametric study of trapezoidal and rectangular corrugation forms has been undertaken to match the experimental studies. The model used is represented by equations (3) to (5). The corrugation height h has been varied between 1 and 10mm, the corrugation angle Φ between 0° and 80°, the lengths b_1 (=b_3) between 1 and 10mm while the laminate thickness t has been kept constant at 0.5mm. In order to establish the elastic structural strain two constraints have been considered. The first one is strain related and ensures that the maximum material strain does not exceed ~60% of the failure material strain of the flat laminate. This was found experimentally to be the elastic limit. The second constraint is a physical geometric constraint that limits the horizontal extension to the theoretical extension that could be achieved by flattening the corrugation. The constraint that gives the lowest value has been taken as being critical.

Figure 6 shows carpet plots of the structural elastic strain and the transverse equivalent elastic modulus for hat-type corrugations (trapezoidal and rectangular) for three fixed values of b_1 against a non-dimensional linear function of h and Φ [23]. The highest strain is achieved for rectangular corrugation (Φ=0°) with high values of h and low values of b_1. Consequently, this same case gives the lowest modulus. On the contrary low values of h and high values of Φ give low strain and high modulus values. It is not so easy to determine what b_1 should be to give highest or lowest strain or modulus. Thus carpet plots from Figure 6 have been combined into a lattice plot (essentially a three-dimensional carpet plot) represented in Figure 7 and Figure 8. They show that, depending on the values of h and Φ, the optimal value for b_1 for maximum/minimum strain/modulus varies. For example, at Φ=0°, b_1 should be small for maximum strain, while if Φ=50°, b_1 should be large for maximum strain.

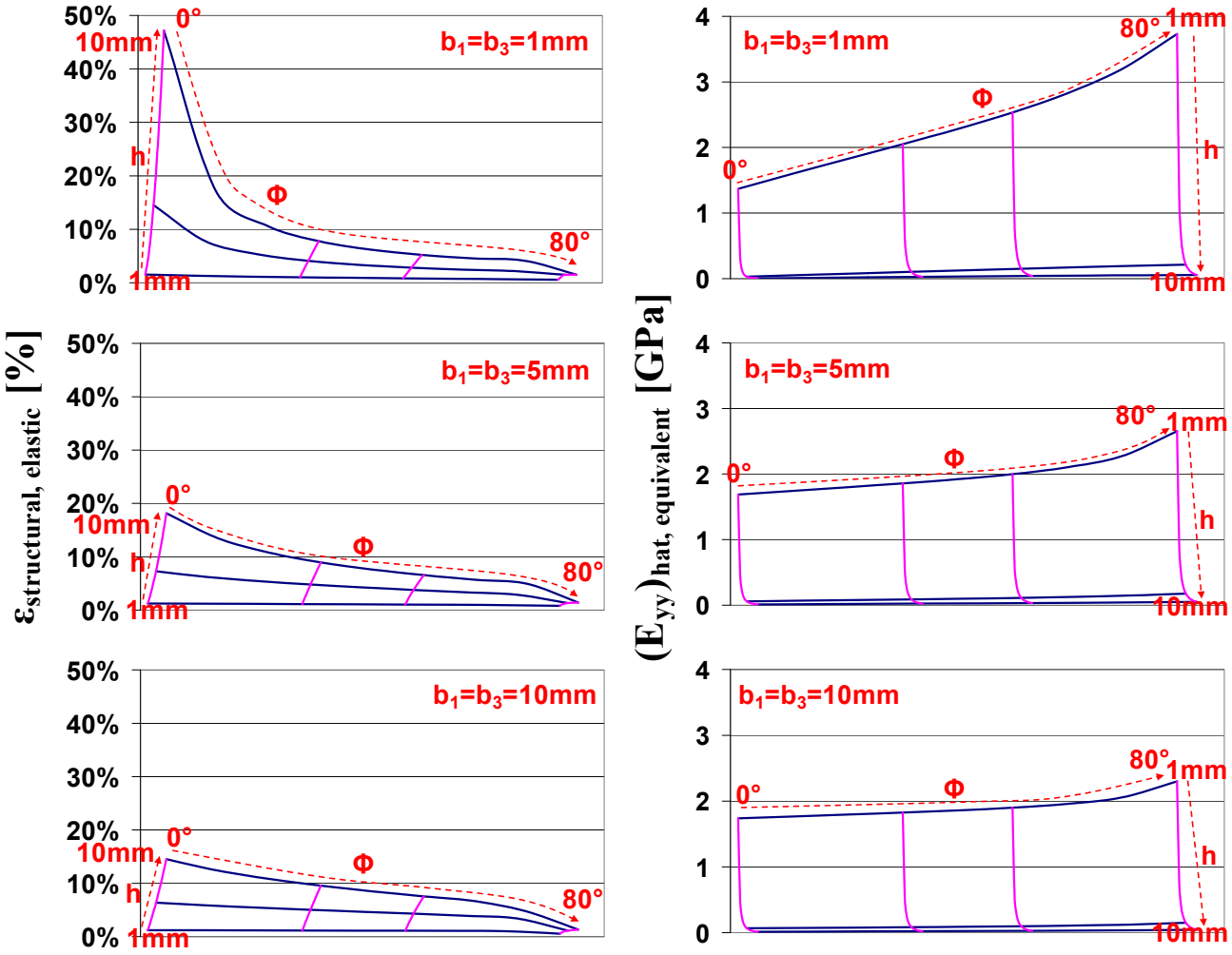

Figure 6: Carpet plots showing the effects of the geometric parameters on the elastic structural strain and the transverse equivalent elastic modulus (plotted according to [23])

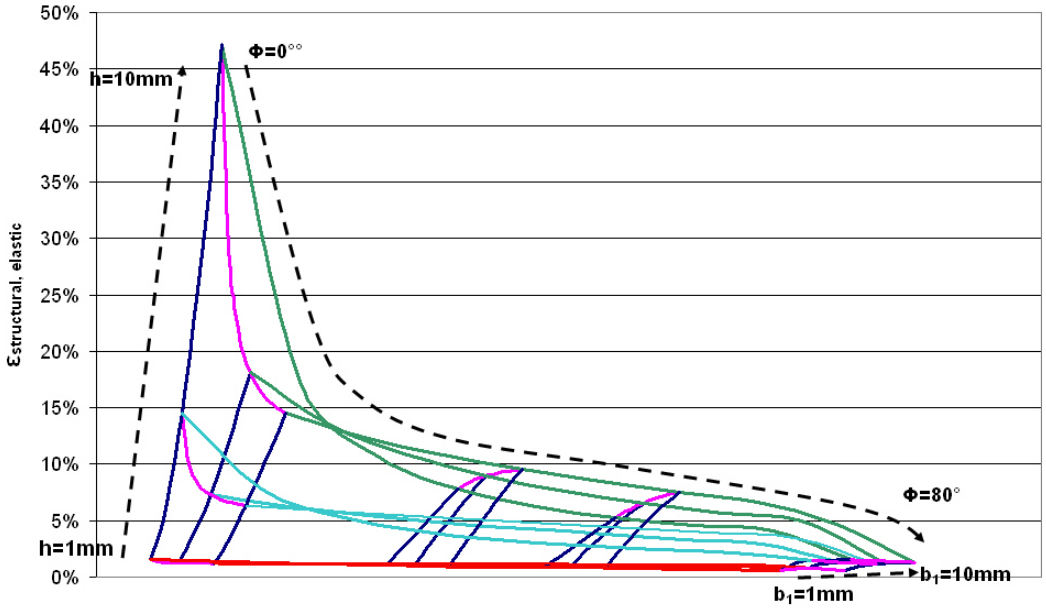

Figure 7: Lattice plot showing the effects of the geometric parameters on the elastic structural strain [23]

The reason for this is that for small Φ the horizontal deflections come mainly from the

inclined/vertical members. Hence, a small b_1 is advantageous to keep the projected length small for large structural strains. However, as Φ initially increases there comes a point at about Φ=20° where the length of b_1 makes no difference to the strain. Then, between 20°<Φ<90°, the proportion of the horizontal deflection of the horizontal member increases and can become larger than the inclined member contribution up to a maximum before it reduces to the case where Φ=90° (flat laminate) and the length of b_1 no longer has any effect. This means that in the regime 20°<Φ<90°, b_1 should be longer to give a maximum contribution to the deflection. The same effect is found for the equivalent elastic modulus e.g. in the regions where b_1 makes the strain large the modulus is low and vice-versa.

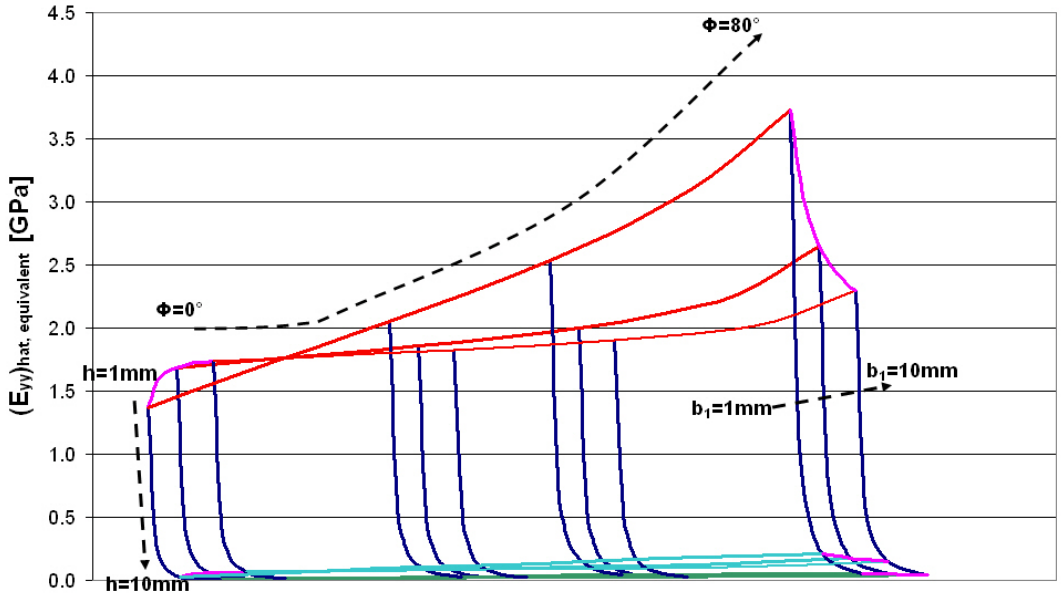

Figure 8: Lattice plot showing the effects of the geometric parameters on the equivalent elastic modulus [23]

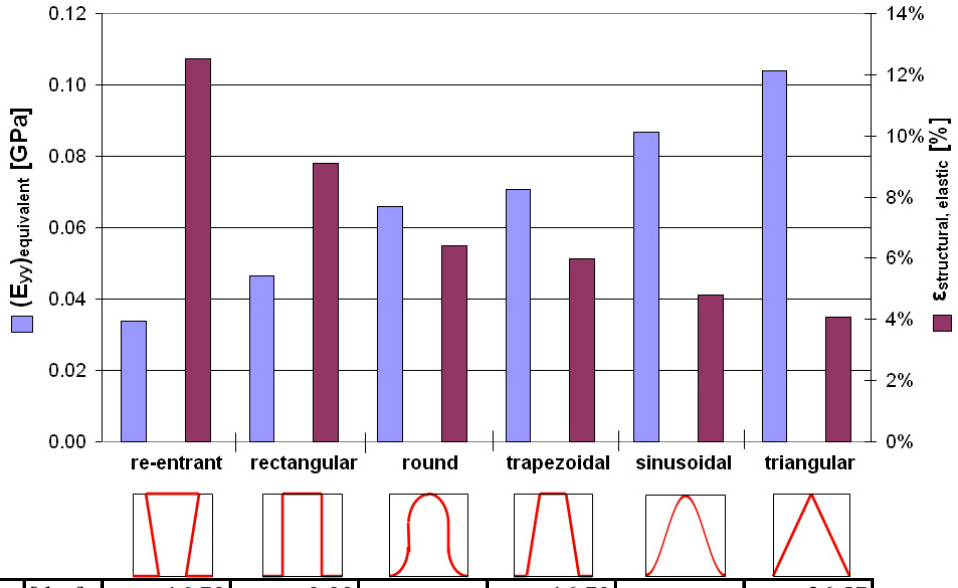

Φ	[deg]	-16.70	0.00	-	16.70	-	26.57
h	[mm]	5.00	5.00	5.00	5.00	5.00	5.00
b_1	[mm]	4.00	2.50	-	1.00	-	0.00
b_3	[mm]	4.00	2.50	-	1.00	-	0.00
w	[mm]	-	-	-	-	2.50	-
s	[mm]	-	-	-	-	5.76	-
r	[mm]	-	-	1.25	-	-	-

Figure 9: Comparison of different corrugation forms in terms of equivalent elastic modulus and structural strain

Figure 6 to Figure 8 show that in general h and Φ have the biggest effect on strain and modulus. An

exception to this rule is the case when Φ is close to zero, whereupon the effects of b_1 become important. While h and Φ influence the amount of bending in the inclined/vertical member of the corrugation, b_1 (and b_3) affect the bending in the horizontal members. Structural strains of up to 50% or equivalent moduli of up to 4GPa are obtained for hat-type corrugations with the present material.
The next stage in this study was to compare different corrugation forms using the models of section 2-4. Using the same constraints as described previously, six different corrugation forms (re-entrant, rectangular, round, trapezoidal, sinusoidal and triangular) have been confined to a 5mm x 5mm boundary and their structural elastic strain and transverse equivalent elastic modulus compared. The results are given in Figure 9 alongside the values of the geometric parameters.
As expected, a corrugation form that gives high strain has a low modulus. The highest structural strain is achieved by re-entrant corrugations while the highest equivalent modulus is achieved using triangular corrugations for given projected dimensions. In practice the maximum strain is related to the length occupied by the corrugation within the fixed boundaries also known as their developed length. This analysis, combined with Figure 6 to Figure 8, provides a preliminary design space for choosing an optimum corrugation geometry and form depending on the requirements of a composite morphing skin.

4. CONCLUSIONS

This study proposes the use of corrugated composite laminates incorporated in a sandwich structure as a morphable wing skin panel for locally reducing the in- and out-of-plane stiffness in the chordwise direction of a wing. Experimental tests were carried out to quantify the elastic tensile modulus and bending stiffness. This was complemented with an analytical analysis that agreed reasonably well. While this investigation was for a particular corrugation geometry and form, a parametric study of the corrugation geometry for a hat-type corrugation showed that structural strains of up to 50% can be realistically achieved if the stiffness is of no primary concern. Conversely, corrugated laminates with a transverse equivalent elastic modulus of about 4GPa can be designed. Furthermore it has been shown that for fixed projected dimensions, re-entrant corrugations give the highest strain while triangular corrugations have the highest modulus. Hence, this leads to conclude that morphing skins including corrugated laminates can be designed within a wide design envelope to suit a particular set of requirements that depend on the intended application.

ACKNOWLEDGEMENTS

The authors would like to thank GE Aviation and the UK EPSRC (Engineering and Physical Sciences Research Council) for their support and funding of this work through the University Technology Strategic Partnership - SMARTCOMP (EP/D03423X/1). Bond (GR/T03383/01) would also like to thank EPSRC for funding his Advanced Research Fellowship.

REFERENCES

1. Thill, C., J. Etches, I. Bond, K. Potter, and P. Weaver, "Morphing skins". *The Aeronautical Journal*, **112**, (1129) pp 117-138 (2008).
2. Moir, I. and A. Seabridge (2008). "Aircraft systems - Mechanical, electrical, and avionics subsytems integration", (3rd edition), John Wiley & Sons Ltd, West Sussex, UK, 2008.
3. Kermode, A.C. (1996). "Mechanics of flight", (10th edition), Longman Group Limited, Essex,

UK, 1996.
4. Rudolph, P.K.C., *High-Lift Systems on Commercial Subsonic Airliners*. 1996, NASA Ames Research Center: Moffet Field, CA, USA.
5. DeCamp, R.W. and R. Hardy. "Mission Adaptive Wing Advanced Research Concepts. 1984. Seattle, WA, USA: AIAA (CP 849), USA 84. 2088, New York, NY, USA.
6. DeCamp, R.W. and R. Hardy, "Mission Adaptive Wing Research Programme". *Aircraft Engineering*, **53**, (1) pp 10-11 (1981).
7. Kudva, J.N., "Overview of the DARPA smart wing project". *Journal of Intelligent Material Systems and Structures*, **15**, (4) pp 261-267 (2004).
8. Kota, S., J.A. Hetrick, and R.F. Osborn Jr, "Adaptive structures: Moving into the mainstream". *Aerospace America*, **44**, (9) pp 16-18 (2006).
9. Sun, H.-H. and J. Spencer, "Buckling strength assessment of corrugated panels in offshore structures". *Marine Structures*, **18**, (7-8) pp 548-565 (2005).
10. Perel, D. and C. Libove, "Elastic Buckling of Infinitely Long Trapezoidally Corrugated Plates in Shear". *Journal of Applied Mechanics*, **45**, (3) pp 579-582 (1978).
11. Shanley, F.R., "Cardboard-Box Wing Structures". *Journal of the Aeronautical Sciences*, **14**, (12) pp 713-715 (1947).
12. Herbert, R.C., P.G. Young, C.W. Smith, R.J. Wootton, and K.E. Evans, "The hind wing of the desert locust (Schistocerca gregaria Forskal) III. A finite element analysis of a deployable structure". *Journal of Experimental Biology*, **203**, (19) pp 2945-2955 (2000).
13. Wootton, R.J., "The mechanical design of insect wings". *Scientific American*, **263**, (5) pp 114-20 (1990).
14. Wootton, R.J., "Functional-Morphology of Insect Wings". *Annual Review of Entomology*, **37**, pp 113-140 (1992).
15. Wootton, R.J., "Support and Deformability in Insect Wings". *Journal of Zoology*, **193**, (Apr) pp 447-468 (1981).
16. Wootton, R.J., K.E. Evans, R. Herbert, and C.W. Smith, "The hind wing of the desert locust (Schistocerca gregaria Forskal) I. Functional morphology and mode of operation". *Journal of Experimental Biology*, **203**, (19) pp 2921-2931 (2000).
17. Yokozeki, T., S. Takeda, T. Ogasawara, and T. Ishikawa, "Mechanical properties of corrugated composites for candidate materials of flexible wing structures". *Composites Part A: Applied Science and Manufacturing*, **37**, (10) pp 1578-1586 (2006).
18. Thill, C., J.A. Etches, I.P. Bond, K.D. Potter, and P. Weaver, *Corrugated composite structures for aircraft morphing skin applications*, in *18th International Conference of Adaptive Structures and Technologies*. 2007: Ottawa, Ontario, Canada.
19. Briassoulis, D., "Equivalent Orthotropic Properties of Corrugated Sheets". *Computers and Structures*, **23**, (2) pp 129-138 (1986).
20. Samanta, A. and M. Mukhopadhyay, "Finite element static and dynamic analyses of folded plates". *Engineering Structures*, **21**, (3) pp 277-287 (1999).
21. Rao, K.P., "Shear Buckling of Corrugated Composite Panels". *Composite Structures*, **8**, (3) pp 207-220 (1987).
22. Weggel, D.C., D.M. Boyajian, and S.-E. Chen, "Modelling structures as systems of springs". *World Transactions on Engineering and Technology Education*, **6**, (1) (2007).
23. ESDU, *Use of carpet plots to represent functions of two variables*. 2003, ESDU 04008.